CHEMISTRY OF MATERIALS

Article

pubs.acs.org/cm

Lithium Extraction Mechanism in Li-Rich Li_2MnO_3 Involving Oxygen Hole Formation and Dimerization

Hungru Chen and M. Saiful Islam*

Department of Chemistry, University of Bath, Bath, BA2 7AY, U.K.

Supporting Information

ABSTRACT: Lithium-rich oxide electrodes with layered structures have attracted considerable interest because they can deliver high energy densities for lithium-ion batteries. However, there is significant debate regarding their redox chemistry. It is apparent that the mechanism of lithium extraction from lithium-rich Li_2MnO_3 is not fully understood, especially in relation to the observed O_2 evolution and structural transformation. Here, delithiation and kinetic processes in Li_2MnO_3 are investigated using *ab initio* simulation techniques employing high level hybrid functionals as they reproduce accurately the electronic structure of oxygen hole states. We show that Li extraction is charge-compensated by oxidation of the oxide anion, so that the overall delithiation reaction involves lattice oxygen loss. Localized holes on oxygen (O^-) are formed as the first step but are not stable leading to oxygen dimerization (with O−O ∼ 1.3 Å) and eventually to the formation of molecular O_2. Oxygen dimerization facilitates Mn migration onto octahedral sites in the vacated lithium layers. The results suggest that reversible oxygen redox without major structural changes is only possible if the localized oxygen holes are stabilized and oxygen dimerization suppressed. Such an understanding is important for the future optimization of new lithium-rich cathode materials for high energy density batteries.

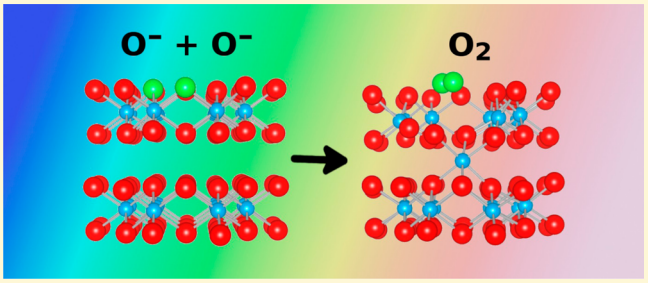

1. INTRODUCTION

Manganese-based oxides have long been studied as cathode materials for lithium-ion batteries,[1−3] with advantages of low cost and nontoxicity over cobalt-based compounds such as $LiCoO_2$. Recently, Li-rich oxide compounds $xLi_2MnO_3{\cdot}(1-x)LiMO_2$, alternatively written as $Li[Li_{x/3}M_{(1-3/x)}]O_2$ (M = Ni, Mn, Co), with layered rock-salt structures have attracted considerable interest because they can deliver high reversible capacities in excess of 250 mAh/g[4−7] after the first activation charge−discharge cycle. However, they suffer from a continuous voltage and capacity fade which hinders their practical application.

A common feature of Li-rich layered oxide cathodes is an irreversible high voltage plateau at around 4.5 V vs Li/Li^+ during the first charge, even after the cation redox limit has been reached. This large extra capacity cannot be accounted for by transition metal oxidation. To explain the electrochemical activity beyond the transition metal redox limit in a Li-rich manganese oxide, Dahn et al.[8] proposed oxygen loss from the crystal lattice as the charge compensation mechanism. Oxygen gas evolution during the first charge has since been observed directly.[9,10]

Li_2MnO_3 is the end member of the Li-rich layered oxides[11−34] which exhibits the characteristic first-charge plateau at 4.5 V. This material was originally considered to be electrochemically inactive because Mn^{4+} ions are not expected to be oxidized further. However, it is now well established that Li can be electrochemically extracted and reinserted.[11−17] A first-charge capacity as large as 452 mAh/g has been reported, corresponding to 98% of lithium extraction from its structure.[18] Both the electrochemical behavior and structure characterization of cycled Li_2MnO_3 indicate the transformation from a layered to a spinel structure,[9−11,15] a process involving Mn cation migration.

As with all Li-rich layered oxides, the origin of the electrochemical activity of Li_2MnO_3 at 4.5 V is not fully understood. Oxygen gas evolution has been observed accompanying lithium extraction from Li_2MnO_3 during the first charge.[9,10,12] However, direct extraction of oxygen ions from the bulk is unlikely due to prohibitively high oxide ion migration barrier energies (>1.5 eV).[20,21] An alternative mechanism of Li ions exchanging with protons that are introduced by electrolyte decomposition has been proposed.[11] Nevertheless, a recent solid-state nuclear magnetic resonance (NMR) study confirmed reversible Li extraction and insertion into the structure without proton exchange.[16]

More recently, there has been significant debate regarding the oxygen redox chemistry of layered Li-rich oxides.[7,35−44] Tarascon et al.[39,43,44] attributed the extra storage capacity in 4d and 5d transition metal oxides (e.g., $Li_2Ru_{1-y}Sn_yO_3$) to the oxidation of O^{2-} to peroxide-like species $(O_2)^{n-}$ and indicated the importance of metal-anion covalency in the oxygen redox

Received: July 13, 2016
Revised: September 5, 2016
Published: September 6, 2016

DOI: 10.1021/acs.chemmater.6b02870
Chem. Mater. 2016, 28, 6656−6663

process. Bruce and co-workers[7] investigated $Li_{1.2}[Ni_{0.13}Co_{0.13}Mn_{0.54}]O_2$ and confirmed that oxygen is lost from the lattice at 4.5 V; they also report that Li removal is charge compensated by localized holes on the oxygen atoms coordinated by Mn^{4+} and Li^+. Ceder and co-workers[45] have examined layered and cation-disordered Li-excess oxides and proposed how specific local Li-excess environments lead to labile oxygen electrons that participate in the practical capacity; they also stress that covalency does not lead to a higher capacity than would be expected from the transition metal alone. Goodenough and co-workers[46] indicate that on oxidation, holes are introduced into the O 2p bands of a layered manganese [IV] oxide; they also show that these oxygen holes are not cycled reversibly and might become trapped in peroxide ions.

It is apparent that the precise mechanism of Li-ion extraction from Li-rich Li_2MnO_3 is not clearly established, especially in relation to the experimentally observed evolution of O_2 and structural transformation. In this work, delithiation reaction enthalpies and kinetic processes in Li_2MnO_3 are studied using hybrid-density functional theory techniques. We show that Li extraction is accompanied by oxygen oxidation but that the oxygen hole (O^-) species are not stable, leading to oxygen dimerization (with O−O ∼ 1.3 Å) and eventually O_2 formation. The results suggest that reversible oxygen redox without major structural change is only possible if the O^- hole can be stabilized and oxygen dimerization suppressed.

2. METHODS

All calculations were performed within the framework of density functional theory (DFT) using the Vienna ab initio simulation package (VASP).[47] In order to obtain accurate chemical reaction energies, electron exchange and correlation were described using the Heyd−Scuseria−Ernzerhof (HSE06) hybrid functional.[48] The HSE06 functional has been shown to reproduce formation enthalpies of metal oxides and yields Li intercalation potentials consistent with experimental values.[49,50] The HSE06 functional also yields a O_2 dimer binding energy of −5.16 eV, in excellent agreement with the experimental value, and gives a good description of electronic properties such as band gaps and oxygen hole states,[51−53] which are essential for describing the oxygen redox chemistry in this study. Future work could also include explicit dispersion terms for interlayer interactions.[54]

Valence electrons were described using a planewave basis set with a cutoff energy of 450 eV. The interactions between valence and core electrons were treated using the projector augmented-wave (PAW) method.[55] The k-space was sampled with a *k*-point mesh with spacings smaller than 0.05 $Å^{-1}$. Spin-polarization effects were included, and ferromagnetic coupling between magnetic manganese cations was assumed.

Surface lithium extraction was modeled using a 9-layer Li_2MnO_3 monoclinic (131) surface slab model, which is equivalent to the rock-salt (001) surface. Each layer was composed of stoichiometric Li_2MnO_3, making this a type I nonpolar surface,[56] and has been calculated to be the most stable surface of layered metal oxides.[57]

Kinetic steps including oxygen dimer formation and Mn migration in delithiated Li_2MnO_3 were modeled using a 2 × 2 × 2 supercell. Activation energies were calculated using the nudged elastic band (NEB) method. The computational methods employed here have been applied successfully to a wide range of lithium battery materials.[58−61]

3. RESULTS AND DISCUSSION

3.1. Crystal Structure and Single Lithium Ion Extraction. The calculations reproduced the observed monoclinic (space group *C*2/*m*) structure of Li_2MnO_3. It can be described as a cation-ordered layered rock-salt structure, consisting of alternating Li and mixed Li and Mn layers, and hence the formula can also be written as $Li[Li_{1/3}Mn_{2/3}]O_2$. Table 1 lists calculated structural data in comparison with experiment. The HSE06 functional reproduces observed lattice parameters and metal−oxygen bond lengths to within 1%. The calculated density of states is included in Supporting Information, Figure S1, which shows strong mixing between Mn-3d and O-2p states with the highest occupied states having a predominant O 2p character. The calculated bulk energy bandgap is 3.7 eV; to the best of our knowledge, there is currently no experimental bandgap available for comparison.

Table 1. Calculated and Experimental[62] Lattice Parameters and Mean Metal−Oxygen Bond Lengths of Li_2MnO_3

length	experiment (Å)	calculation (Å)
a	4.937	4.916
b	8.532	8.491
c	5.030	4.983
Li_{4h}−O	2.102	2.089
Li_{2c}−O	2.102	2.089
Li_{2b}−O	2.060	2.053
Mn−O	1.912	1.898

To understand the charge compensation mechanism upon Li extraction, changes in the electronic structure of Li_2MnO_3 upon extraction of a single Li atom from a surface layer was examined, as this represents the first step of the charging process. Two symmetrically inequivalent lithium sites on the simulated surface were considered (as shown in Figure S2) that lead to different charge compensating behavior. These two sites are referred to as Li-surf-A and Li-surf-B hereafter. For comparison, the extraction of a single Li atom from the bulk was also calculated (i.e., an Li atom from a layer well below the simulated surface, referred to as Li-bulk). The voltage required for the lithium extraction was calculated using the standard approach.[63,64]

The changes in the electronic structure upon extraction of a single Li atom from different crystal sites are illustrated in Figure 1. The density of states plots show that lithium extraction produces localized hole states within the bandgap of Li_2MnO_3. This is in contrast to the metallic behavior after Li removal reported in previous DFT studies.[22,23] Assuming a topotactic solid-solution type of Li extraction reaction without ion migration in Li_2MnO_3, oxygen is predicted to be the main oxidized species from previous static DFT calculations.[20−23] However, the first charge plateau clearly indicates a two-phase type of Li extraction reaction.

The real space charge density associated with the localized hole state created by lithium extraction in each case is also illustrated in Figure 1, from which the oxidized chemical species can be identified. The extraction of a single Li atom from the bulk requires 5.24 V and is accompanied by hole localization on an oxygen adjacent to the vacated Li site, indicating oxygen oxidation $O^{2-} \rightarrow O^- + e^-$ with the formation of an oxygen hole, O^-. Extraction of Li-surf-A is also accompanied by oxygen oxidation but requires a lower potential of 4.56 V.

The difference in oxidation potential between surface and bulk oxygens can be attributed to their different electrostatic environments. It is known that the reaction $O^- + e^- \rightarrow O^{2-}$ in the gaseous phase is endothermic and that the existence of O^{2-} anions in the solid state is due to a stabilizing electrostatic potential created by positively charged cations. Consequently,

DOI: 10.1021/acs.chemmater.6b02870
Chem. Mater. 2016, 28, 6656−6663

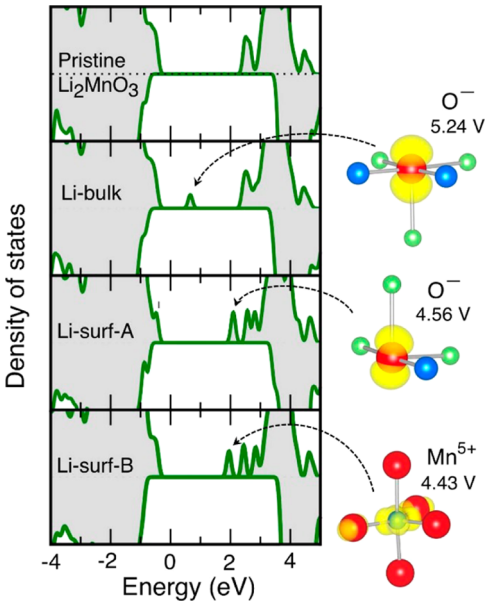

Figure 1. Density of states (DOS) plots for pristine Li_2MnO_3 and for Li_2MnO_3 with one Li atom removed from different sites. The Fermi level is set to 0 eV. Charge densities and redox potentials shown on the right correspond to the hole states marked by arrows in the density of states plots. Red, blue, and green spheres denote oxygen, manganese, and lithium atoms, respectively.

the oxidation potential of O^{2-} in the solid state varies and depends strongly on its site electrostatic environment.[65,66]

To understand the difference in behavior between the surface and the bulk, the electrostatic potential at different oxygen sites were calculated; the results are shown in Figure 2. Owing to a reduced cation coordination number, the electrostatic potential at some surface oxygen sites is higher, i.e., the potential well for an electron is shallower than that in the bulk by more than 1 V. In other words, O^{2-} is less stable at the surface and consequently requires less energy to be oxidized to O^-.

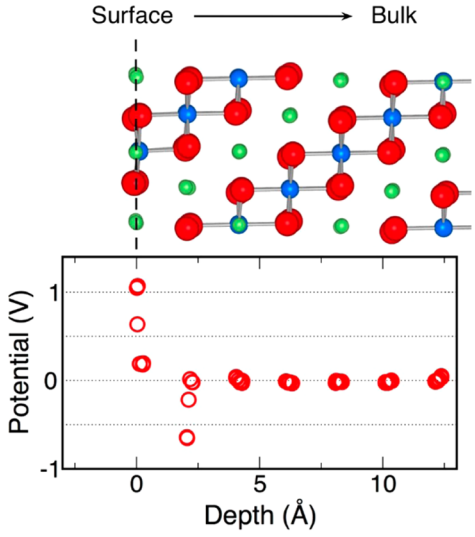

Figure 2. Oxygen site electrostatic potential at different depths from the (131) surface of Li_2MnO_3, as indicated by open circles. The potential in the bulk is set at 0 V. A lower potential corresponds to greater stabilization of electrons. Red, blue, and green spheres denote oxygen, manganese, and lithium atoms, respectively.

The extraction of the Li-surf-B atom produces a slightly lower potential of 4.43 V. This is accompanied by hole localization on a 5-fold coordinate Mn atom at the surface, in which the tetravalent Mn^{4+} ion has been oxidized to the pentavalent ion, Mn^{5+}. Such an oxidation state is unusual, although it should be noted that Mn^{5+} species have been discussed in relation to other manganese oxide battery materials such as Li_3MnO_4, $Li_7Mn(BO_3)_3$, and $Li_4Mn_2O_5$.[67−69] This result is supported by the reduction of its magnetic moment from 2.95 to 2.22 μB, corresponding to a change in electronic configuration from d^3 (Mn^{4+}) to d^2 (Mn^{5+}). The MnO_5 unit also adopts a trigonal bipyramidal geometry with very short Mn−O bonds, as shown in Figure S3. It should be stressed that oxidation to Mn^{5+} is only accessible for 5-coordinate Mn at the surface. Thus, it can only account for a small fraction of the total capacity and is not the main redox process upon Li extraction.

3.2. Overall Delithiation Reaction. The long plateau observed during the first charge of Li_2MnO_3 indicates that delithiation proceeds by a two-phase reaction.[11−13] Here, we examine the redox chemistry of the overall Li extraction reaction. First, the reaction to form MnO_3 without oxygen loss or phase transformation is considered:

$$Li_2MnO_3 \rightarrow 2Li^+ + 2e^- + MnO_3 \quad (1)$$

In this reaction, we find that the calculated magnetic moment on Mn cations in the product MnO_3 has the same value, 2.9 μ_B (Mn^{4+}, d^3), as in Li_2MnO_3, whereas the magnetic moment on two-thirds of the oxygen ions increases from zero in Li_2MnO_3 to 0.8 μ_B in MnO_3. This result indicates the localization of holes on oxygen with the formation of O^- hole species on anion sites closest to the vacated Li sites.

As shown in Figure 3, these localized hole states have a predominately oxygen 2p character, with the lobes of the p orbitals pointing toward the the vacant Li site Li site in the transition metal layer. Hence, Mn ions remain in their

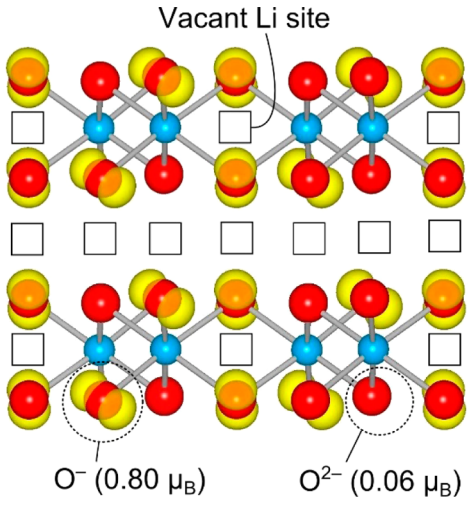

Figure 3. Two different oxygen species O^- and O^{2-} in the delithiated product MnO_3. The yellow isosurface represents the electron density associating with the lowest unoccupied states (hole states). Magnetic moments carried by the two oxygen species are given in brackets. Small nonzero value on O^{2-} is due to Mn-3d/O-2p mixing. Red and blue spheres denote oxygen and manganese atoms, respectively. Oxygen ions surrounded by yellow iso-surfaces are O^-, and the others are O^{2-}.

DOI: 10.1021/acs.chemmater.6b02870
Chem. Mater. 2016, 28, 6656−6663

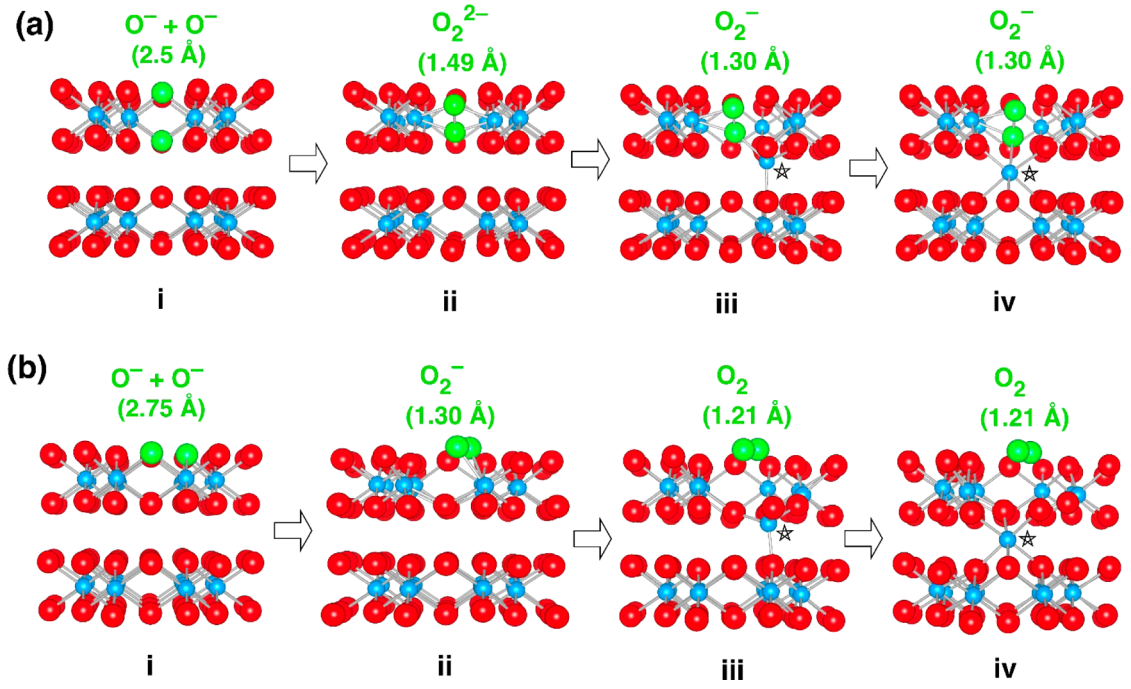

Figure 4. Reaction pathways in bulk MnO_3 toward oxygen dimerization and phase transformation. (a) Pathway A with initial O−O configuration along the *c*- axis. (b) Pathway B with initial O−O configuration in the *ab* plane. Red and blue spheres denote oxygen and manganese atoms, respectively. Green spheres denote oxygen ions that undergo dimerization, and their separation distances are given in parentheses. Migrating Mn atoms are indicated by stars.

tetravalent (d^3) state, and lithium extraction is accompanied by oxidation of O^{2-} to O^-. MnO_3 can therefore be formally written as $(Mn^{4+})(O^{2-})(O^-)_2$.

If delithiation ends with MnO_3 as the final product, then Li extraction from Li_2MnO_3 should be reversible since MnO_3 retains the original layered structure. However, this is not consistent with the experimentally observed structural transformation and oxygen evolution. Moreover, the calculated voltage for this topotactic reaction is 5.07 V, noticeably higher than the experimental lithium extraction potential of 4.5 V.

The simulated delithiation behavior of Li_2MnO_3 is distinctly different from that of Li_2RuO_3 and Li_2IrO_3 that contain 4*d* and 5*d* transition metal ions. In Li_2RuO_3 and Li_2IrO_3, some O−O distances are shortened spontaneously from 2.8 Å to around 2.4 Å upon Li extraction. Although this has been attributed to the formation of O_2^{n-} dimer species,[39,43,44] its exact nature and direct O−O bonding at such a large separation needs further investigation.[70] In contrast, such shortening of the O−O separation does not develop spontaneously in Li_2MnO_3 upon Li extraction from our calculations. It will be demonstrated below that the O−O bond formation in delithiated Li_2MnO_3 is predominantly a kinetic process that requires overcoming an energy barrier.

Next, the lithium extraction reaction accompanied by oxygen loss was considered:

$$Li_2MnO_3 \rightarrow 2Li^+ + 2e^- + MnO_2 + O_2 \quad (2)$$

Here, MnO_2 is assumed to have the λ-MnO_2 spinel structure since this has the same cubic close-packed oxygen sublattice as Li_2MnO_3. In addition, structure characterization and electrochemical measurements suggest transformation from layered Li_2MnO_3 to a spinel-like structure upon cycling.[11,13]

The calculated voltage for reaction 2 is 3.79 V, significantly lower than reaction 1 without oxygen loss. Therefore, reaction 2 is thermodynamically more favorable and consistent with the experimentally observed structural transformation and oxygen evolution.[11−14] Since O_2 is the reaction product, direct O−O bonding or oxygen dimer formation must be involved during the reaction. Reaction 2 can be viewed as reaction 1 followed by the decomposition of MnO_3 according to

$$MnO_3 \rightarrow MnO_2 + \frac{1}{2}O_2 \quad (3)$$

which can also be written as

$$(Mn^{4+})(O^{2-})(O^-)_2 \rightarrow (Mn^{4+})(O^{2-})_2 + \frac{1}{2}O_2 \quad (4)$$

This reaction is found to have a favorable enthalpy of −2.66 eV, a result that again implies that MnO_3 is not the final product of the delithiation process but instead decomposes to MnO_2 and O_2.

We note that the calculated equilibrium voltage for reaction 2 is slightly lower than experimental values. This difference is most likely due to the neglect of an overpotential associated with sluggish chemical reactions with poor kinetics.[71] In any case, our results are consistent with recent studies,[7] which indicate that oxygen redox is often observed in compounds that contain high proportions of Mn^{4+} and Li^+ cations and that there is a balance between O^{2-} redox and oxygen loss.

3.3. Oxygen Dimer Formation and Manganese Migration. Li extraction from Li_2MnO_3 has been demonstrated above to be accompanied by the oxidation of O^{2-} to O^-, leading to the reaction intermediate MnO_3 or $(Mn^{4+})(O^{2-})(O^-)_2$. The O^- hole species is known to be unstable in the solid state. Direct detection of O^- species in metal oxides by EPR has only been reported at liquid-helium temperatures after irradiation.[72] Recent theoretical studies[52,73] have shown the instability of oxygen holes, O^-, against the formation of the

DOI: 10.1021/acs.chemmater.6b02870
Chem. Mater. 2016, 28, 6656−6663

peroxide anion, O_2^{2-}, in metal oxides, that is, the reaction $O^- + O^- \rightarrow O_2^{2-}$, has a negative formation enthalpy. Here, we show that the same oxygen dimer formation also occurs in MnO_3, which initially contains O^- hole species. The formation of an oxygen dimer can then trigger migration of Mn atoms from the transition metal layer to the emptied Li layer.

Two reaction pathways were considered, involving initial O−O configurations along the *c* axis and in the *ab* plane, as shown in Figure 4. The reaction enthalpies and activation energies for each reaction step are illustrated in Figure 5. The simulations included full relaxation of all ions in the structure.

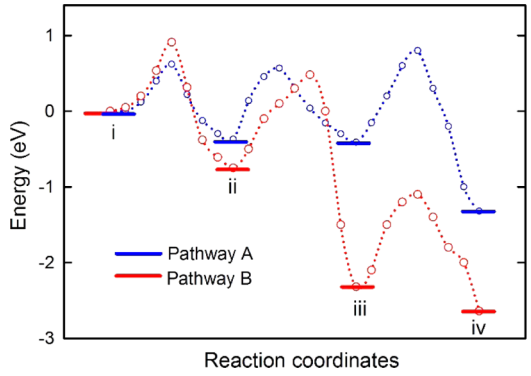

Figure 5. Energy profiles of the reaction pathways A and B shown in Figure 4. The dashed lines indicate energy barriers for the kinetic steps from configurations i to iv. As a reference point, the initial energy is set to 0 eV.

In reaction pathway A, two adjacent O^- hole species in MnO_3 are separated by 2.5 Å across the transition metal layer in the initial configuration. They undergo dimerization and form a nonmagnetic oxygen dimer with an O−O bond length of 1.49 Å, corresponding to a peroxide anion O_2^{2-}. Further support for direct O−O bonding is given by the appearance of bonding and antibonding states in the DOS plots [Figure S4], which are consistent with the molecular orbital diagram of an O_2 molecule.

The reaction enthalpy for this oxygen dimerization process is favorable (−0.37 eV), suggesting that the oxygen dimerization is a thermodynamically driven process. The energy gain is a consequence of direct O−O bonding. Regarding kinetic barriers, the activation energy for the O−O bond formation is calculated to be 0.6 eV. This indicates that despite being lower in energy, the oxygen dimer in delithiated Li_2MnO_3 would not form spontaneously upon structure optimization in static DFT calculations at 0 K; this is because temperature effects are not included and may have been overlooked in previous DFT studies.[21−23,45,74]

The formation of the oxygen dimer O_2^{2-} is followed by the migration of an Mn ion as shown in Figure 4a. The Mn ion initially located on the octahedral site moves to the tetrahedral site above its initial position. Other studies[13,28] including high resolution electron microscopy work have reported local cation migration from the transition metal layer into the Li layer of Li_2MnO_3 and related Li-rich oxides.

The O−O bond length of the oxygen dimer further shortens to 1.30 Å, indicating oxidation from a peroxide O_2^{2-} to superoxide O_2^- species. This is also reflected in the difference in electronic states between O_2^{2-} and O_2^- as shown in Figure S4. Oxidation from peroxide to superoxide requires one extra hole, which is obtained from the reduction of an O^- species back to O^{2-} elsewhere in the crystal.

The final step in reaction pathway A (from configuration iii to iv in Figure 4a) is the migration of the Mn ion on the tetrahedral site to an octahedral site that was originally occupied by Li before delithiation. The oxygen dimer remains a superoxide O_2^- species, and the reaction enthalpy for this step is negative (−0.91 eV). Hence, the overall energy gain for reaction pathway A is 1.32 eV, again suggesting a thermodynamically driven process.

It should be stressed that without oxygen dimer formation, Mn ion migration would not have occurred because the total energy becomes higher (destabilizing the structure) along the same migration path. In other words, Mn ion migration is triggered by oxygen dimer formation.

Figure 4b shows reaction pathway B, which involves the dimerization of two O^- species in MnO_3 that are initially separated by 2.75 Å within the *ab* plane. On the basis of the O−O bond length of 1.30 Å and the electronic structure, the oxygen dimer in configuration ii is identified as a superoxide O_2^- species. Similar to reaction pathway A, the oxygen dimer formation is followed by the migration of an Mn cation from the transition metal layer to a tetrahedral site above its initial site. As the Mn migrates away from the superoxide species, it is further oxidized to a neutral oxygen dimer O_2 with an O−O bond length of 1.21 Å, consistent with the experimental O_2 bond length. In the final step, the tetrahedral Mn then migrates to an octahedral site in the vacant Li layer. All reaction steps in reaction pathway B are exothermic, and the overall energy gain is 2.64 eV.

Comparing the dimerization process in reaction pathways A and B, it appears that the oxygen dimer becomes more oxidized when coordinated by a smaller number of Mn cations. As the neutral O_2 molecule is a more stable species than peroxide O^{2-} and superoxide O^{2-}, owing to its less occupied antibonding π^* orbital, the neutral O_2 molecule should be the final oxidation product. This is consistent with our calculated reaction enthalpies, showing that a configuration with a more oxidized oxygen dimer species is more thermodynamically stable.

The calculated activation energies for oxygen dimer formation and Mn migration are not prohibitively high. Furthermore, these activation energies would decrease at the surface where the coordination number is lower or after subsequent oxygen dimers have formed. If this were not the case, oxygen evolution and structural transformation resulting from Mn migration would not be observed experimentally. Nonetheless, these kinetic steps with energy barriers help to rationalize the slow rate capability during the first charge, as well as the strong temperature dependence of the first charge capacity.

Progression of cooperative oxygen dimer formation and Mn migration will eventually lead to the final delithiation products MnO_2 and O_2. The remaining question is whether the presence of other 3d transition metal cations, such as Ni and Co or cation disordering can stabilize the oxygen holes and give rise to reversible oxygen redox behavior. This issue as well as complex calculations on the effect of the electrolyte at electrode surfaces are topics for future investigation.

4. CONCLUSIONS

Li_2MnO_3 is the end member of the Li-rich layered system $xLi_2MnO_3\cdot(1-x)LiMO_2$, and its redox chemistry on Li extraction has been investigated using DFT simulations. High

DOI: 10.1021/acs.chemmater.6b02870
Chem. Mater. 2016, 28, 6656−6663

level hybrid functionals were used in this work as they reproduce accurately the electronic structure of oxygen hole states. The following key points emerge: (a) Li extraction from Li_2MnO_3 is charge compensated by oxidation of the oxide anion, so that the overall delithiation reaction involves the evolution of O_2 (or lattice oxygen loss) as given by eq 2. (b) Localized holes on oxygen (O^-) are formed as the first step of oxidizing O^{2-}, but the hole species are not thermodynamically stable against dimerization to peroxide O_2^{2-} or superoxide O_2^-. The kinetic barrier for oxygen dimerization is relatively low, suggesting that oxygen holes (O^-) would not survive the time scale of a typical electrochemical reaction at room temperature. Once the oxygen dimer is formed, molecular O_2 is eventually released as a product of delithiation. (c) Oxygen dimerization facilitates Mn migration to the octahedral site in the vacant Li layer which leads to a spinel-like structure. (d) Overall, our results suggest that in order to utilize the oxide ion as a reversible redox center in topotactic electrochemical reactions, it is necessary to stabilize the O^- hole species and prevent oxygen dimerization that can trigger transition metal cation migration and structural transformation. Future work should include improved characterization studies of oxygen hole and peroxide/superoxide species and of gaseous O_2 evolution.

Given the importance of high capacity oxide electrodes, the results presented here provide a greater understanding of lithium extraction and oxygen redox reactions that will help guide the optimization of new Li-rich materials for rechargeable lithium batteries.

■ ASSOCIATED CONTENT

Supporting Information

The Supporting Information is available free of charge on the ACS Publications website at DOI: 10.1021/acs.chemmater.6b02870.

Density of states for Li_2MnO_3; different Li sites on the topmost surface layer of Li_2MnO_3; local geometry around the surface Mn^{5+} species; and local density of states for different oxygen dimer species (PDF)

■ AUTHOR INFORMATION

Corresponding Author

*E-mail: m.s.islam@bath.ac.uk.

Notes

The authors declare no competing financial interest.

■ ACKNOWLEDGMENTS

We gratefully acknowledge support from the EPSRC for the Supergen Energy Storage Hub grant (EP/H019596) and Archer HPC facilities through the Materials Chemistry Consortium (EP/L000202). We thank Dr. Craig Fisher (JFCC Nagoya) and Dr. James Dawson (Bath) for useful discussions.

■ REFERENCES

(1) Thackeray, M. M. Manganese oxides for lithium batteries. *Prog. Solid State Chem.* **1997**, *25*, 1−71.

(2) Zhang, K.; Han, X.; Hu, Z.; Zhang, X.; Tao, Z.; Chen, J. Nanostructured Mn-Based Oxides for Electrochemical Energy Storage and Conversion. *Chem. Soc. Rev.* **2015**, *44*, 699−728.

(3) Manthiram, A.; Chemelewski, K.; Lee, E.-S. A perspective on the high-voltage $LiMn_{1.5}Ni_{0.5}O_4$ spinel cathode for lithium-ion batteries. *Energy Environ. Sci.* **2014**, *7*, 1339−1350.

(4) Thackeray, M. M.; Kang, S.-H.; Johnson, C. S.; Vaughey, J. T.; Benedek, R.; Hackney, S. A. Li_2MnO_3-stabilized LiMO2 (M = Mn, Ni, Co) electrodes for lithium-ion batteries. *J. Mater. Chem.* **2007**, *17*, 3112−3125.

(5) Kim, J.-S.; Johnson, C. S.; Vaughey, J. T.; Thackeray, M. M.; Hackney, S. A.; Yoon, W.; Grey, C. P. Electrochemical and Structural Properties of $xLi_2M'O_3\cdot(1-x)LiMn_{0.5}Ni_{0.5}O_2$ Electrodes for Lithium Batteries (M′ = Ti, Mn, Zr; $0 \leq x \leqslant 0.3$). *Chem. Mater.* **2004**, *16*, 1996−2006.

(6) Shunmugasundaram, R.; Senthil Arumugam, R.; Dahn, J. R. High Capacity Li-Rich Positive Electrode Materials with Reduced First-Cycle Irreversible Capacity Loss. *Chem. Mater.* **2015**, *27*, 757−767.

(7) Luo, K.; Roberts, M. R.; Hao, R.; Guerrini, N.; Pickup, D. M.; Liu, Y.-S.; Edström, K.; Guo, J.; Chadwick, A. V.; Duda, L. C.; Bruce, P. G. Charge-compensation in 3d-transition-metal-oxide intercalation cathodes through the generation of localized electron holes on oxygen. *Nat. Chem.* **2016**, *8*, 684−691.

(8) Lu, Z.; Dahn, J. R. Understanding the Anomalous Capacity of Li/$Li[Ni_xLi_{(1/3-2x/3)}Mn_{(2/3-x/3)}]O_2$ Cells Using In Situ X-Ray Diffraction and Electrochemical Studies. *J. Electrochem. Soc.* **2002**, *149*, A815−A822.

(9) Armstrong, A. R.; Holzapfel, M.; Novák, P.; Johnson, C. S.; Kang, S.-H.; Thackeray, M. M.; Bruce, P. G. Oxygen Loss and Associated Structural Reorganization in the Lithium Battery Cathode $Li[Ni_{0.2}Li_{0.2}Mn_{0.6}]O_2$. *J. Am. Chem. Soc.* **2006**, *128*, 8694−8698.

(10) Castel, E.; Berg, E. J.; El Kazzi, M.; Novák, P.; Villevieille, C. Differential Electrochemical Mass Spectrometry Study of the Interface of $xLi_2MnO_3\cdot(1-x)LiMO_2$ (M = Ni, Co, and Mn) Material as a Positive Electrode in Li-Ion Batteries. *Chem. Mater.* **2014**, *26*, 5051−5057.

(11) Robertson, A. D.; Bruce, P. G. Mechanism of Electrochemical Activity in Li_2MnO_3. *Chem. Mater.* **2003**, *15*, 1984−1992.

(12) Yu, D. Y. W.; Yanagida, K.; Kato, Y.; Nakamura, H. Electrochemical Activities in Li_2MnO_3. *J. Electrochem. Soc.* **2009**, *156*, A417−A424.

(13) Phillips, P. J.; Bareño, J.; Li, Y.; Abraham, D. P.; Klie, R. F. On the Localized Nature of the Structural Transformations of Li_2MnO_3 Following Electrochemical Cycling. *Adv. Energy Mater.* **2015**, *5*, 1501252.

(14) Amalraj, S. F.; Markovsky, B.; Sharon, D.; Talianker, M.; Zinigrad, E.; Persky, R.; Haik, O.; Grinblat, J.; Lampert, J.; Schulz-Dobrick, M.; Garsuch, A.; Burlaka, L.; Aurbach, D. Study of the electrochemical behavior of the "inactive" Li_2MnO_3. *Electrochim. Acta* **2012**, *78*, 32−39.

(15) Kubota, K.; Kaneko, T.; Hirayama, M.; Yonemura, M.; Imanari, Y.; Nakane, K.; Kanno, R. Direct synthesis of oxygen-deficient Li_2MnO_{3-x} for high capacity lithium battery electrodes. *J. Power Sources* **2012**, *216*, 249−255.

(16) Dogan, F.; Croy, J. R.; Balasubramanian, M.; Slater, M. D.; Iddir, H.; Johnson, C. S.; Vaughey, J. T.; Key, B. Solid State NMR Studies of Li_2MnO_3 and Li-Rich Cathode Materials: Proton Insertion, Local Structure, and Voltage Fade. *J. Electrochem. Soc.* **2015**, *162*, A235−A243.

(17) Amalraj, S. F.; Burlaka, L.; Julien, C. M.; Mauger, A.; Kovacheva, D.; Talianker, M.; Markovsky, B.; Aurbach, D. Phase Transitions in Li_2MnO_3 Electrodes at Various States-of-Charge. *Electrochim. Acta* **2014**, *123*, 395−404.

(18) Croy, J. R.; Park, J. S.; Dogan, F.; Johnson, C. S.; Key, B.; Balasubramanian, M. First-Cycle Evolution of Local Structure in Electrochemically Activated Li_2MnO_3. *Chem. Mater.* **2014**, *26*, 7091−7098.

(19) Lanz, P.; Villevieille, C.; Novák, P. Electrochemical activation of Li_2MnO_3 at elevated temperature investigated by in situ Raman microscopy. *Electrochim. Acta* **2013**, *109*, 426−432.

(20) Lee, E.; Persson, K. A. Structural and Chemical Evolution of the Layered Li-Excess Li_xMnO_3 as a Function of Li Content from First-Principles Calculations. *Adv. Energy Mater.* **2014**, *4*, 8.

DOI: 10.1021/acs.chemmater.6b02870
Chem. Mater. 2016, 28, 6656−6663

(21) Hoang, K. Delithiation Mechanism, and Electronic and Ionic Conduction in Layered Lithium Manganese Oxide Cathode Materials. *Phys. Rev. Appl.* **2015**, *3*, 024013.
(22) Koyama, Y.; Tanaka, I.; Nagao, M.; Kanno, R. First-principles study on lithium removal from Li_2MnO_3. *J. Power Sources* **2009**, *189*, 798−801.
(23) Xiao, R.; Li, H.; Chen, L. Density Functional Investigation on Li_2MnO_3. *Chem. Mater.* **2012**, *24*, 4242−4251.
(24) Shin, Y.; Ding, H.; Persson, K. A. Revealing the Intrinsic Li Mobility in the Li_2MnO_3 Lithium-Excess Material. *Chem. Mater.* **2016**, *28*, 2081−2088.
(25) Ye, D. L.; Zeng, G.; Nogita, K.; Ozawa, K.; Hankel, M.; Searles, D. J.; Wang, L. Z. Understanding the Origin of Li_2MnO_3 Activation in Li-Rich Cathode Materials for Lithium-Ion Batteries. *Adv. Funct. Mater.* **2015**, *25*, 7488−7496.
(26) Kim, D.; Lim, J.-M.; Lim, Y.-G.; Park, M.-S.; Kim, Y.-J.; Cho, M.; Cho, K. Understanding of Surface Redox Behaviors of Li_2MnO_3 in Li-Ion Batteries: First-Principles Prediction and Experimental Validation. *ChemSusChem* **2015**, *8*, 3255−3262.
(27) Ruther, R. E.; Dixit, H.; Pezeshki, A. M.; Sacci, R. L.; Cooper, V. R.; Nanda, J.; Veith, G. M. Correlating Local Structure with Electrochemical Activity in Li_2MnO_3. *J. Phys. Chem. C* **2015**, *119*, 18022−18029.
(28) Yan, P.; Xiao, L.; Zheng, J.; Zhou, Y.; He, Y.; Zu, X.; Mao, S. X.; Xiao, J.; Gao, F.; Zhang, J.-G.; Wang, C.-M. Probing the Degradation Mechanism of Li_2MnO_3 Cathode for Li-Ion Batteries. *Chem. Mater.* **2015**, *27*, 975−982.
(29) Jacob, C.; Jian, J.; Su, Q.; Verkhoturov, S.; Guillemette, R.; Wang, H. Electrochemical and Structural Effects of In Situ Li_2O Extraction from Li_2MnO_3 for Li-Ion Batteries. *ACS Appl. Mater. Interfaces* **2015**, *7*, 2433−2438.
(30) Wu, Q.; Maroni, V. A.; Gosztola, D. J.; Miller, D. J.; Dees, D. W.; Lu, W. A Raman-Based Investigation of the Fate of Li_2MnO_3 in Lithium- and Manganese-Rich Cathode Materials for Lithium Ion Batteries. *J. Electrochem. Soc.* **2015**, *162*, A1255−A1264.
(31) Lim, J.-M.; Kim, D.; Lim, Y.-G.; Park, M.-S.; Kim, Y.-J.; Cho, M.; Cho, K. The origins and mechanism of phase transformation in bulk Li_2MnO_3: first-principles calculations and experimental studies. *J. Mater. Chem. A* **2015**, *3*, 7066−7076.
(32) Sayle, T. X. T.; Caddeo, F.; Monama, N.; Kgatwane, K. M.; Ngoepeb, P. E.; Sayle, D. C. Origin of electrochemical activity in nano-Li_2MnO_3; stabilization via a 'point defect scaffold'. *Nanoscale* **2015**, *7*, 1167−1180.
(33) Kubobuchi, K.; Mogi, M.; Ikeno, H.; Tanaka, I.; Imai, H.; Mizoguchi, T. Mn L-2,L-3-edge X-ray absorption spectroscopic studies on charge-discharge mechanism of Li_2MnO_3. *Appl. Phys. Lett.* **2014**, *104*, 053906.
(34) Wang, R.; He, X.; He, L.; Wang, F.; Xiao, R.; Gu, L.; Li, H.; Chen, L. Atomic Structure of Li_2MnO_3 after Partial Delithiation and Re-Lithiation. *Adv. Energy Mater.* **2013**, *3*, 1358−1367.
(35) Muhammad, S.; Kim, H.; Kim, Y.; Kim, D.; Song, J. H.; Yoon, J.; Park, J.-H.; Ahn, S.-J.; Kang, S.-H.; Thackeray, M. M.; Yoon, W.-S. Evidence of reversible oxygen participation in anomalously high capacity Li- and Mn-rich cathodes for Li-ion batteries. *Nano Energy* **2016**, *21*, 172−184.
(36) Hy, S.; Liu, H.; Zhang, M.; Qian, D.; Hwang, B.-J.; Meng, Y. S. Performance and design considerations for lithium excess layered oxide positive electrode materials for lithium ion batteries. *Energy Environ. Sci.* **2016**, *9*, 1931−1954.
(37) Shimoda, K.; Minato, T.; Nakanishi, K.; Komatsu, H.; Matsunaga, T.; Tanida, H.; Arai, H.; Ukyo, Y.; Uchimoto, Y.; Ogumi, Z. Oxidation behaviour of lattice oxygen in Li-rich manganese-based layered oxide studied by hard X-ray photoelectron spectroscopy. *J. Mater. Chem. A* **2016**, *4*, 5909−5916.
(38) Cao, T.; Shi, C.; Zhao, N.; He, C.; Li, J.; Liu, E. Understanding the Electrochemical Properties of Li-Rich Cathode Materials from First-Principles Calculations. *J. Phys. Chem. C* **2015**, *119*, 28749−28756.
(39) McCalla, E.; Abakumov, A. M.; Saubanere, M.; Foix, D.; Berg, E. J.; Rousse, G.; Doublet, M.-L.; Gonbeau, D.; Novak, P.; Van Tendeloo, G.; Dominko, R.; Tarascon, J.-M. Visualization of O-O peroxo-like dimers in high-capacity layered oxides for Li-ion batteries. *Science* **2015**, *350*, 1516−1521.
(40) Oishi, M.; Yogi, C.; Watanabe, I.; Ohta, T.; Orikasa, Y.; Uchimoto, Y.; Ogumi, Z. Direct observation of reversible charge compensation by oxygen ion in Li-rich manganese layered oxide positive electrode material, $Li_{1.16}Ni_{0.15}Co_{0.19}Mn_{0.50}O_2$. *J. Power Sources* **2015**, *276*, 89−94.
(41) Buchholz, D.; Li, J.; Passerini, S.; Aquilanti, G.; Wang, D.; Giorgetti, M. X-ray Absorption Spectroscopy Investigation of Lithium-Rich, Cobalt-Poor Layered-Oxide Cathode Material with High Capacity. *ChemElectroChem* **2015**, *2*, 85−97.
(42) Koga, H.; Croguennec, L.; Menetrier, M.; Mannessiez, P.; Weill, F.; Delmas, C. Different oxygen redox participation for bulk and surface: A possible global explanation for the cycling mechanism of $Li_{1.20}Mn_{0.54}CO_{0.13}Ni_{0.13}O_2$. *J. Power Sources* **2013**, *236*, 250−258.
(43) Sathiya, M.; Rousse, G.; Ramesha, K.; Laisa, C. P.; Vezin, H.; Sougrati, M. T.; Doublet, M. L.; Foix, D.; Gonbeau, D.; Walker, W.; Prakash, A. S.; Ben Hassine, M.; Dupont, L.; Tarascon, J. M. Reversible anionic redox chemistry in high-capacity layered-oxide electrodes. *Nat. Mater.* **2013**, *12*, 827−835.
(44) Saubanere, M.; McCalla, E.; Tarascon, J. M.; Doublet, M. L. The intriguing question of anionic redox in high-energy density cathodes for Li-ion batteries. *Energy Environ. Sci.* **2016**, *9*, 984−991.
(45) Seo, D.-H.; Lee, J.; Urban, A.; Malik, R.; Kang, S. Y.; Ceder, G. The structural and chemical origin of the oxygen redox activity in layered and cation-disordered Li-excess cathode materials. *Nat. Chem.* **2016**, *8*, 692−697.
(46) Du, K.; Zhu, J.; Hu, G.; Gao, H.; Li, Y.; Goodenough, J. B. Exploring reversible oxidation of oxygen in a manganese oxide. *Energy Environ. Sci.* **2016**, *9*, 2575−2577.
(47) Kresse, G.; Furthmüller, J. Efficient iterative schemes for *ab initio* total-energy calculations using a plane-wave basis set. *Phys. Rev. B: Condens. Matter Mater. Phys.* **1996**, *54*, 11169−11186.
(48) Heyd, J.; Scuseria, G. E.; Ernzerhof, M. Erratum: "Hybrid functionals based on a screened Coulomb potential" [J. Chem. Phys.118, 8207 (2003)]. *J. Chem. Phys.* **2006**, *124*, 219906.
(49) Chevrier, V. L.; Ong, S. P.; Armiento, R.; Chan, M. K. Y.; Ceder, G. Hybrid density functional calculations of redox potentials and formation energies of transition metal compounds. *Phys. Rev. B: Condens. Matter Mater. Phys.* **2010**, *82*, 075122.
(50) Franchini, C.; Podloucky, R.; Paier, J.; Marsman, M.; Kresse, G. Ground-state properties of multivalent manganese oxides: Density functional and hybrid density functional calculations. *Phys. Rev. B: Condens. Matter Mater. Phys.* **2007**, *75*, 195128.
(51) Varley, J. B.; Janotti, A.; Franchini, C.; Van de Walle, C. G. Role of self-trapping in luminescence and *p*-type conductivity of wide-band-gap oxides. *Phys. Rev. B: Condens. Matter Mater. Phys.* **2012**, *85*, 081109.
(52) Chen, H.; Umezawa, N. Hole localization, migration, and the formation of peroxide anion in perovskite $SrTiO_3$. *Phys. Rev. B: Condens. Matter Mater. Phys.* **2014**, *90*, 035202.
(53) Chen, H.; Dawson, J. A. Molecular Oxygen as Charge-Compensating and Magnetic Centers in Anatase TiO_2. *Phys. Rev. Appl.* **2015**, *3*, 064011.
(54) Aykol, M.; Kim, S.; Wolverton, C. van der Waals Interactions in Layered Lithium Cobalt Oxides. *J. Phys. Chem. C* **2015**, *119*, 19053−19058.
(55) Blöchl, P. E. Projector augmented-wave method. *Phys. Rev. B: Condens. Matter Mater. Phys.* **1994**, *50*, 17953−17979.
(56) Tasker, P. W. The stability of ionic crystal surfaces. *J. Phys. C: Solid State Phys.* **1979**, *12*, 4977.
(57) Kramer, D.; Ceder, G. Tailoring the Morphology of $LiCoO_2$: A First Principles Study. *Chem. Mater.* **2009**, *21*, 3799−3809.
(58) Armstrong, A. R.; Lyness, C.; Panchmatia, P.; Islam, M. S.; Bruce, P. G. The lithium intercalation process in the low voltage lithium battery anode $Li_{1+x}V_{1-x}O_2$. *Nat. Mater.* **2011**, *10*, 223−229.

DOI: 10.1021/acs.chemmater.6b02870
Chem. Mater. 2016, 28, 6656−6663

(59) Eames, C.; Islam, M. S. Ion Intercalation into Two-Dimensional Transition-Metal Carbides: Global Screening for New High-Capacity Battery Materials. *J. Am. Chem. Soc.* **2014**, *136*, 16270−16276.
(60) Armstrong, A. R.; Kuganathan, N.; Islam, M. S.; Bruce, P. G. Structure and Lithium Transport Pathways in Li_2FeSiO_4 Cathodes for Lithium Batteries. *J. Am. Chem. Soc.* **2011**, *133*, 13031−13035.
(61) Deng, Y.; Eames, C.; Chotard, J.-N.; Lalere, F.; Seznec, V.; Emge, S.; Pecher, O.; Grey, C. P.; Masquelier, C.; Islam, M. S. Structural and Mechanistic Insights into Fast Lithium-Ion Conduction in Li_4SiO_4-Li_3PO_4 Solid Electrolytes. *J. Am. Chem. Soc.* **2015**, *137*, 9136−9145.
(62) Boulineau, A.; Croguennec, L.; Delmas, C.; Weill, F. Reinvestigation of Li_2MnO_3 Structure: Electron Diffraction and High Resolution TEM. *Chem. Mater.* **2009**, *21*, 4216−4222.
(63) Aydinol, M. K.; Kohan, A. F.; Ceder, G.; Cho, K.; Joannopoulos, J. *Ab initio* study of lithium intercalation in metal oxides and metal dichalcogenides. *Phys. Rev. B: Condens. Matter Mater. Phys.* **1997**, *56*, 1354−1365.
(64) Islam, M. S.; Fisher, C. A. J. Lithium and sodium battery cathode materials: computational insights into voltage, diffusion and nanostructural properties. *Chem. Soc. Rev.* **2014**, *43*, 185−204.
(65) Harding, J. H.; Pyper, N. C. The meaning of the oxygen second-electron affinity and oxide potential models. *Philos. Mag. Lett.* **1995**, *71*, 113−121.
(66) Walsh, A.; Butler, K. T. Prediction of Electron Energies in Metal Oxides. *Acc. Chem. Res.* **2014**, *47*, 364−372.
(67) Saint, J. A.; Doeff, M. M.; Reed, J. Synthesis and electrochemistry of Li_3MnO_4: Mn in the + 5 oxidation state. *J. Power Sources* **2007**, *172*, 189−19.
(68) Roos, J.; Eames, C.; Wood, S. M.; Whiteside, A.; Islam, M. S. Unusual Mn coordination and redox chemistry in the high capacity borate cathode $Li_7Mn(BO_3)_3$. *Phys. Chem. Chem. Phys.* **2015**, *17*, 22259−22265.
(69) Freire, M.; Kosova, N. V.; Jordy, C.; Chateigner, D.; Lebedev, O. I.; Maignan, A.; Pralong, V. A new active Li-Mn-O compound for high energy density Li-ion batteries. *Nat. Mater.* **2016**, *15*, 173−177.
(70) Alvarez, S.; Hoffmann, R.; Mealli, C. A Bonding Quandary—or—A Demonstration of the Fact That Scientists Are Not Born With Logic. *Chem. - Eur. J.* **2009**, *15*, 8358−8373.
(71) Hong, W. T.; Risch, M.; Stoerzinger, K. A.; Grimaud, A.; Suntivich, J.; Yang, S.-H. Toward the rational design of non-precious transition metal oxides for oxygen electrocatalysis. *Energy Environ. Sci.* **2015**, *8*, 1404−1427.
(72) Abraham, M. M.; Chen, Y.; Unruh, W. P. Formation and stability of V^- and V Al centers in MgO. *Phys. Rev. B* **1974**, *9*, 1842−1852.
(73) Chen, S.; Wang, L.-W. Double-hole-induced oxygen dimerization in transition metal oxides. *Phys. Rev. B: Condens. Matter Mater. Phys.* **2014**, *89*, 014109.
(74) Okamoto, Y. Ambivalent Effect of Oxygen Vacancies on Li_2MnO_3: A First-Principles Study. *J. Electrochem. Soc.* **2012**, *159*, A152−A157.

DOI: 10.1021/acs.chemmater.6b02870
Chem. Mater. 2016, 28, 6656−6663